

# Constraints on the curvature of the Universe and dynamical dark energy from the full-shape and BAO data

Anton Chudaykin,<sup>1,\*</sup> Konstantin Dolgikh,<sup>2,†</sup> and Mikhail M. Ivanov<sup>3,1,‡</sup>

<sup>1</sup>*Institute for Nuclear Research of the Russian Academy of Sciences,  
60th October Anniversary Prospect, 7a, 117312 Moscow, Russia*

<sup>2</sup>*M.V. Lomonosov Moscow State University,  
Vorobjevy Gory, 119991 Moscow, Russia*

<sup>3</sup>*Center for Cosmology and Particle Physics, Department of Physics,  
New York University, New York, NY 10003, USA*

We present limits on the parameters of the  $\Lambda$ CDM,  $w_0$ CDM, and  $w_0w_a$ CDM models obtained from the joint analysis of the full-shape, baryon acoustic oscillations (BAO), big bang nucleosynthesis (BBN) and supernovae data. Our limits are fully independent of the data on the cosmic microwave background (CMB) anisotropies, but rival the CMB constraints in terms of parameter error bars. We find the spatial curvature consistent with a flat universe  $\Omega_k = -0.043^{+0.036}_{-0.036}$  (68% C.L.); the dark-energy equation of state parameter  $w_0$  is measured to be  $w_0 = -1.031^{+0.052}_{-0.048}$  (68% C.L.), consistent with a cosmological constant. This conclusion also holds for the time-varying dark energy equation of state, for which we find  $w_0 = -0.98^{+0.099}_{-0.11}$  and  $w_a = -0.33^{+0.63}_{-0.48}$  (both at 68% C.L.). The exclusion of the supernovae data from the analysis does not significantly weaken our bounds. This shows that using a single external BBN prior, the full-shape and BAO data can provide strong CMB-independent constraints on the non-minimal cosmological models.

## 1. INTRODUCTION AND SUMMARY

Elucidating the geometry of the Universe and the nature of the late-time expansion are some of the key goals of current and planned cosmological observations. The current data is consistent with the picture that the universe is flat and the late-time expansion can be described by a small cosmological constant [1]. These are the key assumptions of the base flat  $\Lambda$ CDM model, whose parameters are accurately measured by the Planck CMB data [2]. The deviations from this model are strongly constrained by the combination of the Planck data with baryon acoustic oscillations (BAO) and, optionally, the supernovae data [1].

It has been recently shown that the parameters of the base  $\Lambda$ CDM model can be independently determined with the galaxy full-shape (FS) data<sup>1</sup> [5–7] collected by

the Baryon Acoustic Oscillation Spectroscopic Survey (BOSS) [8]. This has become possible due to a significant progress in large-scale structure theory achieved in the last decade with the development of the effective field theory of large scale structure (see [5, 6] and references therein). The full-shape data also sharpens the constraints on various extensions of the  $\Lambda$ CDM model:  $\nu\Lambda$ CDM,  $\nu\Lambda$ CDM+ $N_{\text{eff}}$  [9, 10],  $w_0$ CDM [11], and the early dark energy [12, 13]. But crucially, it can even replace the CMB data in constraining beyond- $\Lambda$ CDM scenarios. An example is the minimal dynamical dark energy model  $w_0$ CDM [11], whose parameters can be determined from the big bang nucleosynthesis (BBN), BOSS FS, BAO and supernovae (SNe) data. In this paper we continue testing non-minimal cosmological models with this data set, focusing on  $\Lambda$ CDM,  $w_0$ CDM and  $w_0w_a$ CDM models. Compared to Ref. [11], we extend the BOSS full-shape data by including the hexadecapole moment of the redshift-space power spectrum in the analysis, although, quite surprisingly, we found that it does not appreciably shrink the posterior contours even in the beyond- $\Lambda$ CDM scenarios.

Deriving CMB-independent constraints on the  $\Lambda$ CDM,  $w_0$ CDM and  $w_0w_a$ CDM models is important for multiple reasons. The CMB data already provided tight con-

\* [chudy@ms2.inr.ac.ru](mailto:chudy@ms2.inr.ac.ru)

† [dolgikh.ka15@physics.msu.ru](mailto:dolgikh.ka15@physics.msu.ru)

‡ [mi1271@nyu.edu](mailto:mi1271@nyu.edu)

<sup>1</sup> Our notion of the full-shape analysis should not be confused with the terminology of Ref. [3], which studies how a fixed shape template gets distorted by the Alcock-Paczynski effect [4]. In contrast, we use the power spectrum shape itself to constrain the physical cosmological parameters.

straints on the parameters of these models. However, the CMB temperature likelihoods are known to be affected by various anomalies. In particular, the large-scale part of the spectrum exhibits the so-called “low- $\ell$  deficit” - suppression of the power for angular multipole numbers  $20 \lesssim \ell \lesssim 30$ . Besides that, late-time matter clustering determines the lensing smoothing of the acoustic peaks, whose observed amplitude is known to exceed the prediction of the  $\Lambda$ CDM model by over  $2\sigma$  [1]. This is the so-called “lensing anomaly”, which prefers models with enhanced large-scale structure growth, e.g. a Universe with a positive spatial curvature [1, 14]. These anomalies have been intensely investigated in the past works, which showed that most likely they are just statistical fluctuations [1, 15–17]. Nevertheless, the presence of these anomalies makes it desirable to have additional constraints from independent data sets.

In this paper, we infer the parameters of the  $\text{o}\Lambda\text{CDM}$ ,  $w_0\text{CDM}$  and  $w_0w_a\text{CDM}$  models from a joint fit to the BOSS DR12 full shape data, supplemented with the BBN prior on the physical baryon density  $\omega_b$ , the BAO data from BOSS and eBOSS, and the Pantheon type Ia supernovae (SNe) measurements. Our main result is that this data set is able to strongly constrain the parameters of the considered non-minimal models:

$$\begin{cases} \Omega_k = -0.043_{-0.036}^{+0.036}, & \text{o}\Lambda\text{CDM, FS+BAO+SNe}, \\ w_0 = -1.031_{-0.048}^{+0.052}, & w_0\text{CDM, FS+BAO+SNe}, \\ \begin{cases} w_0 = -0.98_{-0.11}^{+0.10} \\ w_a = -0.32_{-0.48}^{+0.63} \end{cases} & w_0w_a\text{CDM, FS+BAO+SNe}. \end{cases} \quad (1)$$

Our limit on the spatial curvature of the Universe is comparable to the Planck TT+lowE measurement,  $\Omega_k = -0.056_{-0.018}^{+0.028}$ . However, it is significantly weaker than the combined Planck+BAO+SNe limit. Still, our constraint on  $\Omega_k$  is one of the strongest CMB-independent bounds present in the literature.

The FS+BAO+SNe data set is very competitive with the CMB for the dynamical dark energy models. Our error bars on the parameters  $w_0$  and  $w_0 - w_a$  are only  $\sim 30\%$  weaker than those from the Planck CMB + BAO + SNe data analysis [1]:  $w_0 = -1.028 \pm 0.032$  ( $w_0\text{CDM}$ ),  $w_0 = -0.961 \pm 0.077$ ,  $w_a = -0.28_{-0.27}^{+0.31}$  ( $w_0w_a\text{CDM}$ ).

The key ingredient of our analysis is the BOSS full-shape likelihood introduced in Ref. [5]. Given the BBN prior on  $\omega_b$ , the shape of the galaxy power spectrum provides us with a geometry-independent constraint on the

physical dark matter density  $\omega_{cdm}$ . This fixes the sound horizon at decoupling and allows us to extract the geometric distances from the BAO measurements. These distances can be converted into the parameters controlling the expansion history: the Hubble constant  $H_0$ , the effective spatial curvature density fraction  $\Omega_k$ , the dark energy abundance  $\Omega_{de}$ , along with the equation of state parameters  $w_0, w_a$ . We have found nearly the same value of the sound horizon at the drag epoch  $r_d$  in all models that we consider in this work:

$$r_d = (146 \pm 2.4) \text{ Mpc}. \quad (2)$$

Remarkably, placing strong constraints on the expansion history is possible even without the SNe data. In particular, the BAO+FS measurements from BOSS and eBOSS, supplemented with a single BBN prior, are enough to define the parameters of the  $w_0\text{CDM}$  and  $w_0w_a\text{CDM}$  models,

$$\begin{cases} w_0 = -1.038_{-0.082}^{+0.1}, & w_0\text{CDM, FS+BAO}, \\ \begin{cases} w_0 = -0.81_{-0.34}^{+0.25} \\ w_a = -0.94_{-0.83}^{+1.3} \end{cases}, & w_0w_a\text{CDM, FS+BAO}. \end{cases} \quad (3)$$

All in all, our parameters limits for the  $w_0\text{CDM}$  and  $w_0w_a\text{CDM}$  models are comparable to those obtained from the combination of the Planck CMB, BAO and SNe data, whilst the  $\Omega_k$  constraint is competitive with the primary Planck result, but is weaker than the full Planck + BAO limit. The limits presented in this paper are some of the strongest CMB-dependent constraints on the  $\text{o}\Lambda\text{CDM}$ ,  $w_0\text{CDM}$ ,  $w_0w_a\text{CDM}$  models.

It is important to note that the full-shape data allows us to accurately determine all relevant parameters of the  $\text{o}\Lambda\text{CDM}$ ,  $w_0\text{CDM}$  and  $w_0w_a\text{CDM}$  models. In particular, we find the present-day Hubble constant  $H_0$  consistent with the Planck base  $\Lambda\text{CDM}$  value  $H_0 \simeq 68 \text{ km/s/Mpc}$ , with few percent error bars. The optimal value of  $H_0$  is very robust to the considered extensions of  $\Lambda\text{CDM}$ , which shows that it can be accurately measured from the full-shape and the BAO data in a nearly model-independent way.

The remainder of this paper is structured as follows. We start with the discussion of our data sets in Sec. 2. Sec. 3 contains our main results. Finally, we draw conclusions in Sec. 4. We present the validation of our pipeline on mock catalogs in Appendix A.

## 2. DATA AND METHODOLOGY

### 2.1. Data sets

**Full-shape.** We use the multipoles of the redshift-space power spectrum of the luminous red galaxies observed by BOSS [8]. The power spectrum multipoles were measured from the publicly available catalogs with the `nbodykit` code [18]. The full-shape data is split in four non-overlapping chunks: low- $z$  and high- $z$ , north and south galactic caps. The effective redshifts are  $z_{\text{eff}} = 0.38$  for the low- $z$  samples and  $z_{\text{eff}} = 0.61$  for the high- $z$  samples. We use the data cuts  $[0.01, 0.2] h/\text{Mpc}$ , which are robust w.r.t. higher-order nonlinear corrections omitted in our theory model, see Appendix A for more detail. We fit the full-shape data using one-loop perturbation theory implemented in the `CLASS-PT` code [19]. We use covariance matrices from Patchy mocks [20], which were shown to be robust w.r.t. stochastic noise biases [21, 22]. Further details on our theory models, covariance matrices and the window function treatment can be found in Refs. [5, 19, 21]. Compared to these works, we also include the hexadecapole moment in our analysis. We present the details of our hexadecapole treatment and validation on mocks in Appendix A.

**BAO.** We use the BAO measurements from the post-reconstructed power spectra of the BOSS DR12 data [23], which are covariant with the full-shape data from the pre-reconstruction power spectrum. We analyze these data sets with the methodology of Ref. [24]. Namely, we compute the anisotropic BAO parameters from mock catalogs and the BOSS data using the theoretical error approach [25]. Then auto-covariance of the BAO parameters and their cross-covariance with the power spectrum multipoles is estimated from Patchy mocks [20].

Additionally, we use the small- $z$  BAO measurements from 6DF ( $z_{\text{eff}} = 0.106$ ) [26] and SDSS DR7 MGS ( $z_{\text{eff}} = 0.15$ ) [27], along with the high redshift ( $z_{\text{eff}} = 2.33$ ) Lyman- $\alpha$  forest auto-correlation and the cross-correlation with quasars from eBOSS DR16 [28, 29]. For completeness, we also use the BAO measurements from the eBOSS quasar sample ( $z_{\text{eff}} = 1.48$ ) [30] and the emission line galaxy sample ( $z_{\text{eff}} = 0.845$ ) [31], even though their impact on the eventual parameter constraints is quite marginal. We do not use the BAO from the eBOSS LRG sample [32] because it overlaps with the tail of the BOSS DR12 high- $z$  galaxy sample, which is already con-

tained in our joint full-shape-BAO likelihood for this data chunk.

**Supernovae.** We will use the cosmological supernovae Ia measurements from the Pantheon sample [33].

**BBN.** We will use the BBN measurements from helium and deuterium [34, 35] that constrain the current physical density of baryons  $\omega_b$ . Specifically, we use the results of the “standard” analysis (see footnote 14 of Ref. [5] for more detail), implemented as a following Gaussian prior:

$$\omega_b \sim \mathcal{N}(0.02268, 0.00038^2). \quad (4)$$

### 2.2. Models

We will consider three extensions of the  $\Lambda\text{CDM}$  model:  $\text{o}\Lambda\text{CDM}$ ,  $w_0\text{CDM}$  and  $w_0w_a\text{CDM}$ , in the notation of Refs. [29]. These models share the following set of parameters:<sup>2</sup>

$$\{\omega_b, \omega_{cdm}, h, A_s, n_s\}, \quad (5)$$

where  $\omega_b, \omega_{cdm}$  are the current physical densities of baryons and dark matter,  $h$  is the dimensionless Hubble constant ( $H_0 = h \cdot 100 \text{ km/s/Mpc}$ ), whereas  $A_s$  and  $n_s$  are the amplitude and tilt of the power spectrum of primordial scalar fluctuations. Following [1], we approximate the neutrino sector with one single massive state of mass  $m_\nu = 0.06 \text{ eV}$ .

The main difference between the models we consider shows up in the late-time expansion. The Friedman equation for these models read

$$\begin{aligned} H^2 &= H_0^2 (\Omega_m(1+z)^3 + \Omega_\Lambda + \Omega_k(1+z)^2) & (\text{o}\Lambda\text{CDM}) \\ H^2 &= H_0^2 \left( \Omega_m(1+z)^3 + \Omega_{\text{de}}(1+z)^{3(1+w_0)} \right) & (w_0\Lambda\text{CDM}) \\ H^2 &= H_0^2 \left( \Omega_m(1+z)^3 + \Omega_{\text{de}}(1+z)^{3(1+w_0 + \frac{w_a z}{1+z})} \right) & (w_0w_a\Lambda\text{CDM}) \end{aligned} \quad (6)$$

<sup>2</sup> Note that we fix the current CMB monopole temperature  $T_0$  to the COBE/FIRAS best-fit value  $T_0 = 2.7255 \text{ K}$  [36].  $T_0$  has to be specified because it is an input parameter in the Boltzmann code `CLASS` that we use here [37]. This choice is not crucial for our analysis.  $T_0$  is irrelevant for the thermal history, but affects the late-time expansion through the contribution to the Friedman equation [38]. Given that, in principle, we could measure  $T_0$  from the full-shape and BAO data, but we prefer to use the FIRAS prior because it is very robust and has been independently confirmed by other probes.

where  $\Omega_m, \Omega_\Lambda, \Omega_{\text{de}}$  are the current energy fractions of matter, cosmological constant and dynamical dark energy, respectively, whereas  $\Omega_k$  is the effective energy fraction of the spatial curvature.  $\Omega_k > 0$  corresponds to an open universe (negative curvature),  $\Omega_k < 0$  describes a closed universe (positive curvature). We will jointly fit the combined likelihood with all relevant cosmological parameters (5), supplemented with  $\Omega_k$  (for  $\text{o}\Lambda\text{CDM}$ ),  $w_0$  (for  $w_0\text{CDM}$ ) and  $w_0, w_a$  ( $w_0w_a\text{CDM}$ ).

### 2.3. Role of the full-shape data

Before presenting results of our analysis, let us briefly discuss the role of the full-shape data. To that end, it is instructive to start with the example of the minimal  $\Lambda\text{CDM}$  model. The shape of the galaxy power spectrum yields measurements of  $\omega_b$  and  $\omega_{\text{cdm}}$  through the scale-independent features, such as the relative ratios of the BAO peaks to the broadband slope [5, 39, 40]. Even though a measurement of  $\omega_b$  from the full-shape data is, in principle, possible, the current limits are quite loose [9, 10], which is why we prefer to use the BBN prior on  $\omega_b$ . Combining it with the shape, one can measure the comoving sound horizon at the drag epoch, which can be expressed as [41],

$$r_d = \frac{55.148}{(\omega_{\text{cdm}} + \omega_b)^{0.25351} \omega_b^{0.12807}} \text{Mpc}. \quad (7)$$

The sound horizon helps break the degeneracy with the distance to the galaxies present in the angular scale of the acoustic horizon  $\theta_{\text{BAO}} = r_d/D_V(z_{\text{gal}})$  and the angle of the matter-radiation equality scale  $\theta_{\text{eq}} = 1/(k_{\text{eq}}D_V(z_{\text{gal}}))$ , where  $k_{\text{eq}}$  is the conformal momentum of the perturbations entering the horizon at the matter-radiation equality, and  $D_V$  is the so-called comoving volume-averaged distance [8, 29]. In the  $\Lambda\text{CDM}$  model the only remaining undetermined parameter is the Hubble constant, and hence the measurement of  $D_V$  places a bound directly on  $H_0$ .

The situation becomes more complicated when we consider extensions of  $\Lambda\text{CDM}$  with more parameters defining the late-time background expansion. In this case, there appears a geometric degeneracy which is similar to the geometric degeneracy of the CMB spectrum [42]. In principle, this degeneracy can be broken at the level of the full-shape data by means of the Alcock-Paczynski effect [4], but this is a rather weak effect [5]. In particular

it can only help constrain the background parameters of the  $\Lambda\text{CDM}$  model with BAO when multiple redshifts are combined [1, 41, 43, 44]. However, when we combine the full-shape with the BAO data at different redshifts (assuming a BBN prior), the acoustic horizon is fixed by the shape such that all the distance information can be translated into the remaining background parameters. In the context of the  $w_0\text{CDM}$  model this has been explicitly demonstrated in Ref. [11].

In principle, some information on the expansion history also comes from the large-scale structure growth, but its measurements are quite uncertain due to the galaxy bias and large cosmic variance errors on the quadrupole and hexadecapole measurements [11]. Therefore, the bulk of our constraints is coming from the power spectrum monopole, which gives us  $\omega_{\text{cdm}}$  and  $D_V$ . Hence, we expect our limits to be robust w.r.t. possible contamination by the tensorial anisotropic assembly bias [45], which affects the quadrupole and hexadecapole data. We leave a more detailed analysis of this effect for future work.

We stress that the crucial piece of information is the full-shape measurement of  $\omega_{\text{cdm}}$ , which does not depend on the expansion model. However, it is affected by other parameters defining the shape, e.g. the primordial power spectrum tilt  $n_s$ . Given this reason, we vary this parameter in our analysis, even though the eventual constraints are  $\sim \times 10$  weaker than those from the Planck CMB data. Still, we believe that it is more appropriate to treat  $n_s$  as a free parameter for the purpose of our analysis to derive the constraints independent from the CMB anisotropies.

## 3. RESULTS

In this section we present the results of our MCMC analyses for the considered models. In what follows we will suppress BBN in the notations of our data set, assuming that it is always included by default, i.e. FS+BAO should be understood as FS+BAO+BBN.

### 3.1. $\text{o}\Lambda\text{CDM}$

The triangle plot for the parameters of the  $\text{o}\Lambda\text{CDM}$  model is shown in Fig. 1, the 1d marginalized constraints are presented in the 2nd and 3rd columns of Table I for the FS+BAO and FS+BAO+SNe datasets. The first relevant observation is that the constraints on the shape

Dataset Param.	FB, $\omega\Lambda$ CDM	FBS, $\omega\Lambda$ CDM	FB, $w_0$ CDM	FBS, $w_0$ CDM	FB, $w_0w_a$ CDM	FBS, $w_0w_a$ CDM
	$\omega_{cdm}$	$0.1269^{+0.0087}_{-0.011}$	$0.1273^{+0.0086}_{-0.011}$	$0.1236^{+0.0082}_{-0.0099}$	$0.1233^{+0.0083}_{-0.0096}$	$0.126^{+0.0085}_{-0.01}$
$h$	$0.6948^{+0.015}_{-0.016}$	$0.6945^{+0.013}_{-0.015}$	$0.69^{+0.018}_{-0.021}$	$0.6885^{+0.013}_{-0.014}$	$0.6775^{+0.026}_{-0.026}$	$0.6896^{+0.013}_{-0.014}$
$\ln(10^{10} A_s)$	$2.64^{+0.20}_{-0.20}$	$2.65^{+0.20}_{-0.20}$	$2.77^{+0.17}_{-0.17}$	$2.77^{+0.16}_{-0.16}$	$2.72^{+0.17}_{-0.17}$	$2.72^{+0.17}_{-0.17}$
$n_s$	$0.9153^{+0.068}_{-0.067}$	$0.9136^{+0.068}_{-0.065}$	$0.9334^{+0.066}_{-0.064}$	$0.9346^{+0.065}_{-0.064}$	$0.9191^{+0.066}_{-0.065}$	$0.9236^{+0.066}_{-0.065}$
$\Omega_k$	$-0.044^{+0.043}_{-0.044}$	$-0.043^{+0.036}_{-0.036}$	—	—	—	—
$w_0$	—	—	$-1.038^{+0.1}_{-0.082}$	$-1.031^{+0.052}_{-0.048}$	$-0.805^{+0.25}_{-0.34}$	$-0.9826^{+0.099}_{-0.11}$
$w_a$	—	—	—	—	$-0.9451^{+1.3}_{-0.83}$	$-0.3264^{+0.63}_{-0.48}$
$\Omega_\Lambda$	$0.733^{+0.044}_{-0.044}$	$0.731^{+0.033}_{-0.033}$	—	—	—	—
$\Omega_m$	$0.3109^{+0.013}_{-0.014}$	$0.3119^{+0.012}_{-0.013}$	$0.3087^{+0.015}_{-0.016}$	$0.3091^{+0.011}_{-0.012}$	$0.3262^{+0.023}_{-0.031}$	$0.3121^{+0.012}_{-0.013}$
$\Omega_{de}$	—	—	$0.692^{+0.015}_{-0.015}$	$0.691^{+0.011}_{-0.011}$	$0.674^{+0.031}_{-0.022}$	$0.688^{+0.012}_{-0.012}$
$\sigma_8$	$0.708^{+0.043}_{-0.048}$	$0.708^{+0.043}_{-0.048}$	$0.718^{+0.043}_{-0.048}$	$0.718^{+0.043}_{-0.048}$	$0.705^{+0.044}_{-0.049}$	$0.711^{+0.044}_{-0.049}$
$r_d$ [Mpc]	$146^{+2.4}_{-2.4}$	$146^{+2.4}_{-2.4}$	$146^{+2.4}_{-2.4}$	$146^{+2.4}_{-2.4}$	$146^{+2.4}_{-2.4}$	$146^{+2.4}_{-2.4}$

TABLE I. Mean values and 68% CL minimum credible intervals for the parameters of the various extended models for two data sets differing by the presence of the supernovae data. FB denotes the combination FS+BAO, FBS denotes the combination FS+BAO+SNe. The BBN prior on  $\omega_b$  is assumed in all analyses, and the corresponding posterior is not displayed because it is prior-dominated. The top group represents the parameters that were directly varied in the MCMC chains. The bottom group are the derived parameters.

and amplitude parameters  $\omega_{cdm}, n_s, A_s$  and  $\sigma_8$  in the  $\omega\Lambda$ CDM model are similar to those from the flat  $\Lambda$ CDM model [5] (see also Appendix A). This is consistent with the fact that the shape constraints do not depend on projection effects [9]. The second relevant observation is that the spatial curvature is consistent with zero within 95%CL. Remarkably, the FS+BAO and FS+BAO+SNe data yield a very significant evidence for the cosmological constant even in the presence of the non-zero spatial curvature in the fit.

Comparing the FS+BAO (‘FB’) and FS+BAO+SNe (‘FBS’) cases, we see that the addition of the SNe data improves the  $\Omega_k$  constraint only by  $\sim 20\%$ . This shows that the curvature constraints are indeed dominated by the FS+BAO data sets. Comparing our results to the BAO-only measurements of  $\Omega_k$  and  $\Omega_m$  [29], we see that the addition of the FS data shrinks the error bars by a factor of  $\sim 3$ . Moreover, it allows us to measure  $H_0$  to 2% accuracy, which would not be possible with the BAO-only data.

Let us discuss the implications for the Planck spatial curvature measurements. It is known that the primary Planck data favors the model with positive spa-

tial curvature; i.e. the Planck 2018 TT+low E likelihood prefers a closed universe with more than  $2\sigma$  significance,  $\Omega_k = -0.056^{+0.028}_{-0.018}$  [1]. Our measurement is consistent with this estimate, although the error bars are large enough to enclose the  $\Omega_k = 0$  within  $2\sigma$  as well. The Planck preference for positive spatial curvature can be traced back to the lensing anomaly, which is, most likely, just a statistical fluke [1]. Indeed, the combined Planck+BAO+SNe dataset gives  $\Omega_k = -0.0001 \pm 0.0018$ , consistent with the flat  $\Lambda$ CDM model.

It is worth mentioning that there exist other independent estimates of the spatial curvature of the Universe from different combinations of the SH0ES distance ladder measurements [14], strong lensing time-delays, BAO, BBN, cosmic chronometers and quasar luminosity distances, see [46] and references therein. The strongest one is obtained from the combination BAO+SNe+BBN+SH0ES,  $\Omega_k = -0.091 \pm 0.037$  [14]. This limit is, however, crucially depends on the inclusion of the SH0ES  $H_0$  prior [47], which is in tension with other data sets [48], and hence, this limit should be taken with a grain of salt until the tension is resolved. The error bars from other CMB-independent measurements of

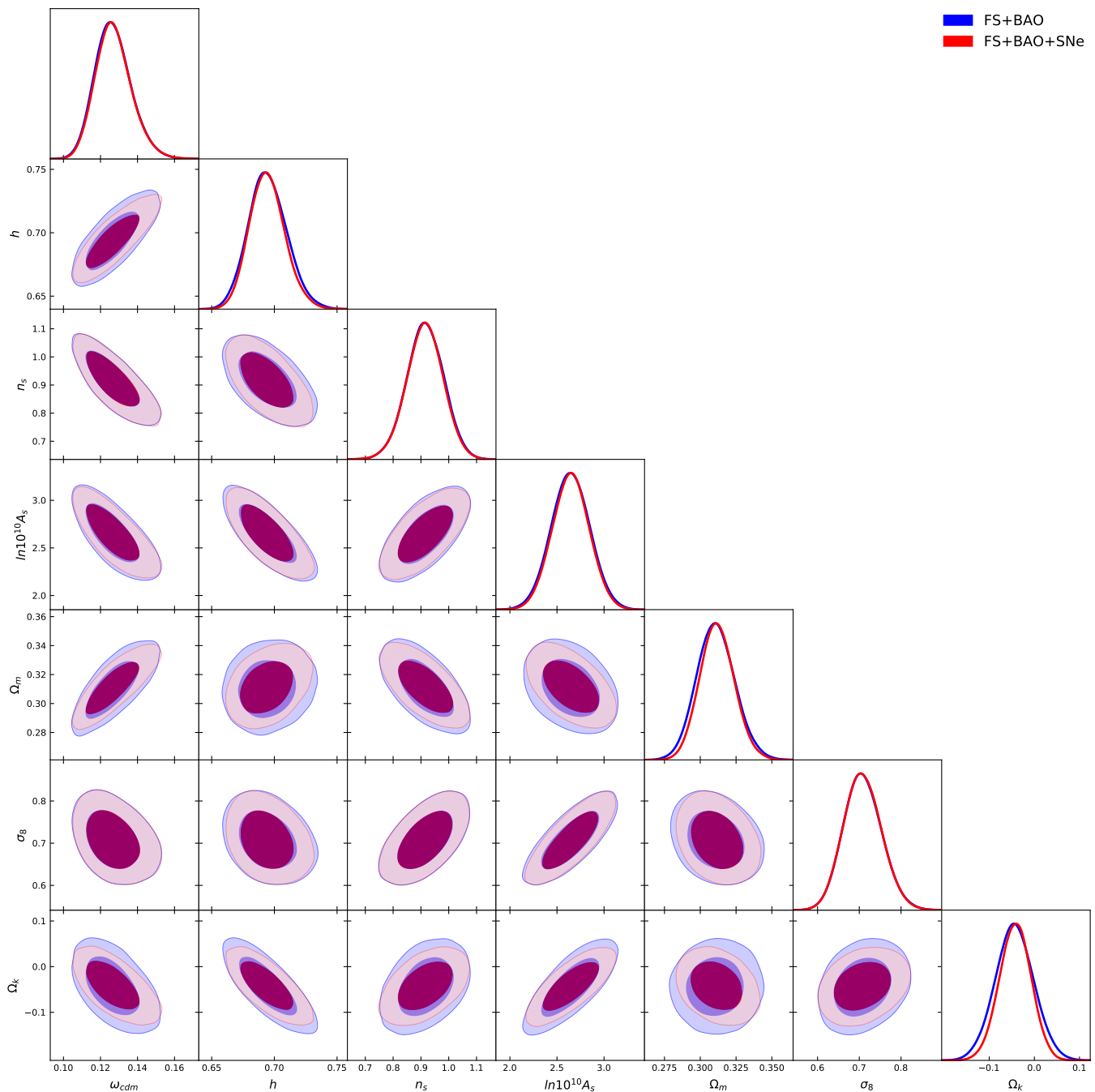


FIG. 1. Posterior distributions of the cosmological parameters of the  $\text{o}\Lambda\text{CDM}$  model.

$\Omega_k$  are at least four times larger than the uncertainty of our measurement.

### 3.2. $w_0\text{CDM}$

Now let us focus on the  $w_0\text{CDM}$  model. Planck-alone prefers very negative  $w_0$ . The triangle plot for the pa-

rameters of the  $\text{o}\Lambda\text{CDM}$  model is shown in Fig. 2, the 1d marginalized constraints are presented in the 4th and 5th columns of Table I for the FS+BAO and FS+BAO+SNe data. The FS+BAO data yields the dark energy equation of state parameter compatible with the cosmological constant value at 68%CL. This can be contrasted with the Planck TT+low E constraints (see chapter 17.1 of [49])

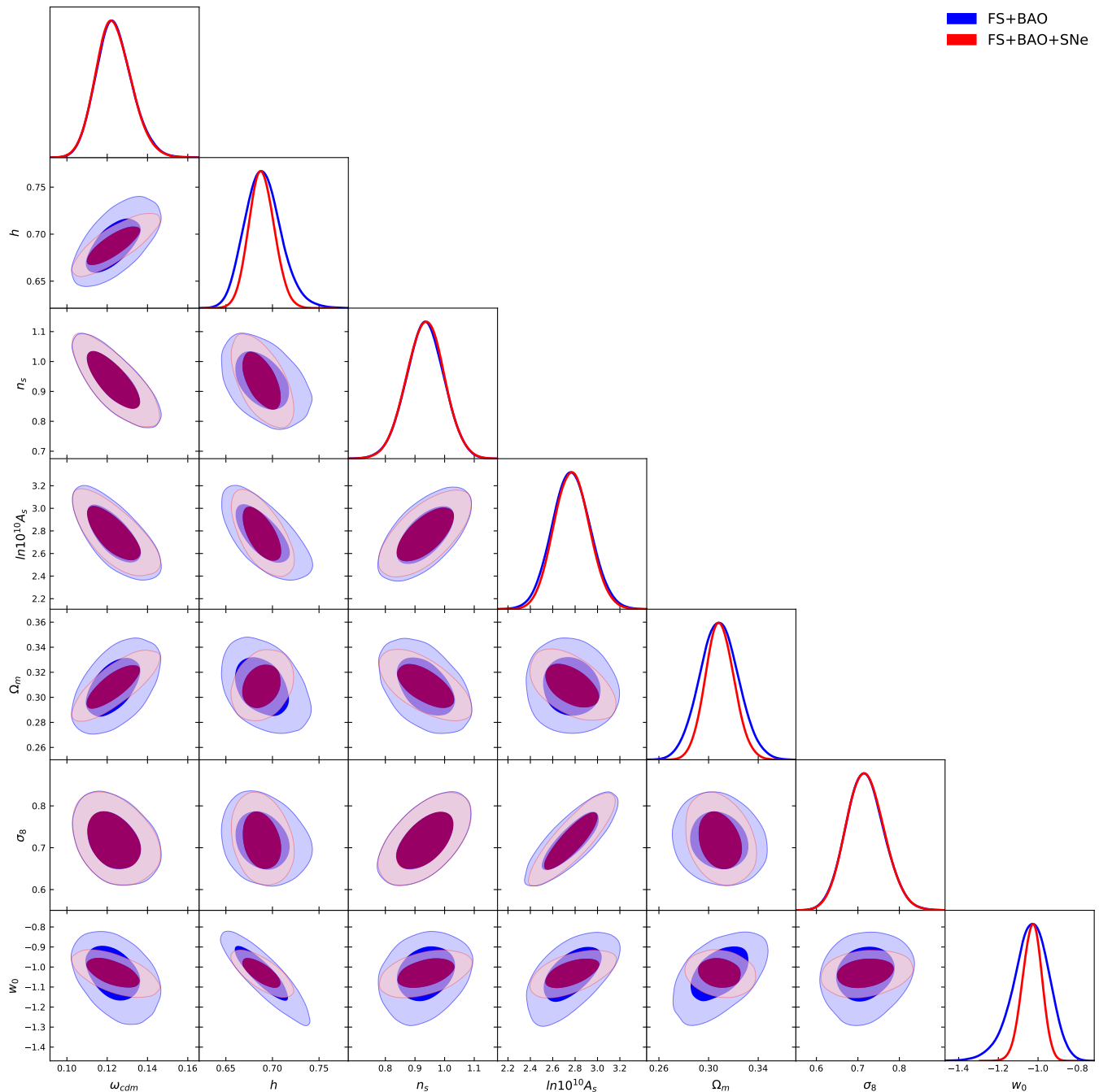


FIG. 2. Posterior distributions of the cosmological parameters of the  $w_0$ CDM model.

$w_0 = -1.56^{+0.19}_{-0.39}$  preferring a  $\sim 2\sigma$  shift of  $w_0$  into the phantom domain.

Our FS+BAO constraint is almost twice stronger than the BAO-only result  $w_0 = -0.69 \pm 0.15$  [29], which is also shifted away from the cosmological constant prediction.

Our final constraints from the FS+BAO+SNe data set are somewhat weaker (by  $\sim 30\%$ ), but still competitive

with the Planck+BAO+SNe result  $w_0 = -1.028 \pm 0.032$ . It is also useful to compare our results with the pioneering analysis of the  $w_0$ CDM model [11] with the FS+BAO+SNe data. This analysis was based on the same data set as ours, the only difference is the addition of the hexadecapole moment in the present work, along with a small update in the eBOSS BAO likelihood. We

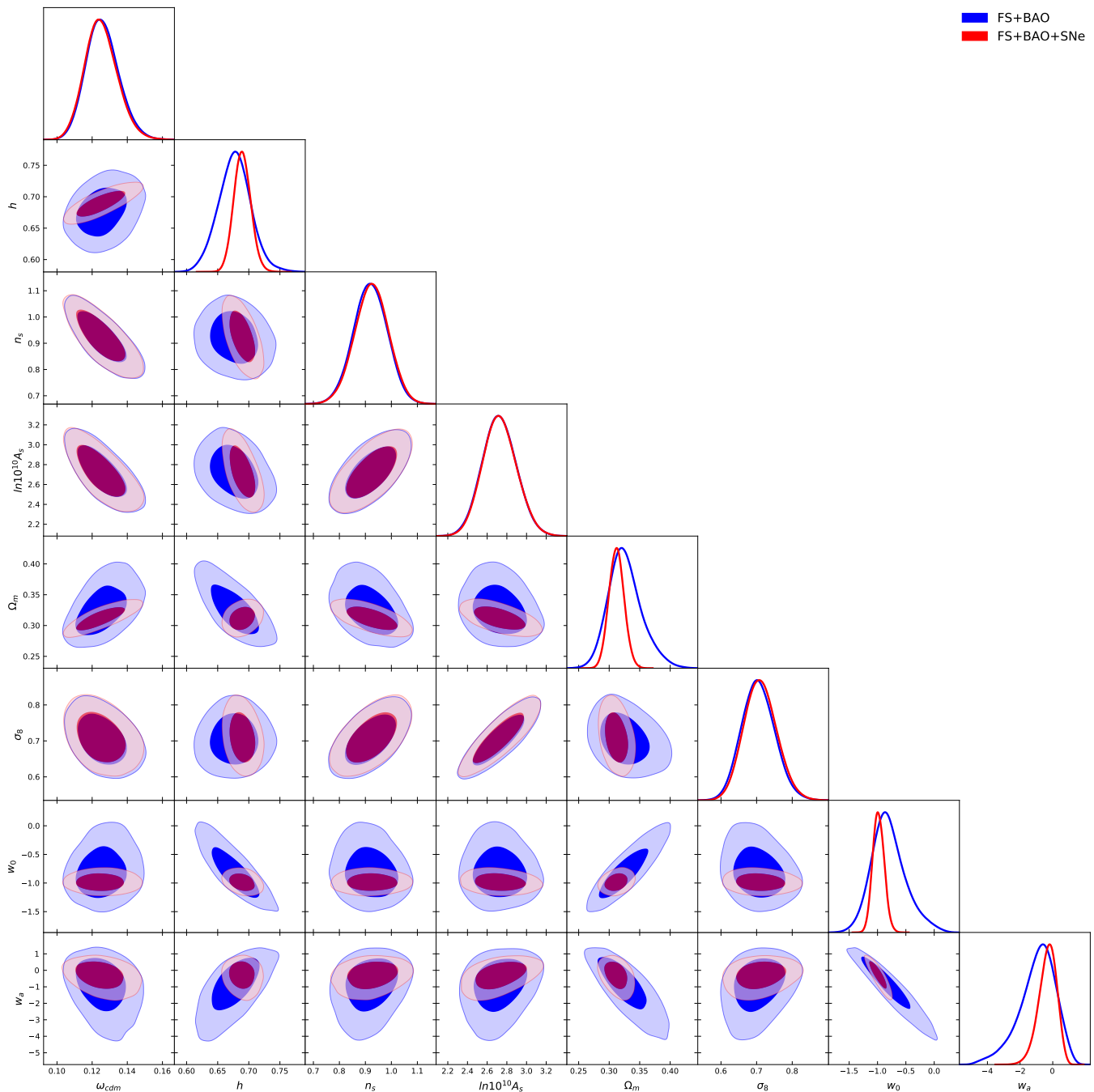


FIG. 3. Posterior distributions of the cosmological parameters of the  $w_0w_a$ CDM model.

observe that this reduces the error bar on  $w_0$  by  $\simeq 30\%$  in the FS+BAO case and by  $\sim 10\%$  in the FS+BAO+SNe case.

### 3.3. $w_0w_a$ CDM

Finally, let us discuss the  $w_0w_a$ CDM model. The triangle plot for the parameters of the  $\text{o}\Lambda$ CDM model is shown in Fig. 3, the 1d marginalized constraints are presented in the 6th and 7th columns of Table I for the FS+BAO and FS+BAO+SNe data.

Our constraints on  $w_0w_a$ CDM model from FS+BAO are comparable to the constraints from different combinations of the primary Planck data with the BAO [49]. In particular, the strongest combination including CMB lensing yields  $w_0 = -0.59 \pm 0.27$ ,  $w_a = -1.24 \pm 0.74$ , which is only  $\sim 10\%$  better than our FS+BAO estimate. The situation somewhat changes with the inclusion of the SNe, which noticeably shrinks the constraints from Planck+BAO to the level  $w_a = -0.961 \pm 0.077$ ,  $w_0 = -0.28^{+0.31}_{-0.27}$ . Our limits on  $(w_0, w_a)$  from the FS+BAO+SNe data are (20%, 40%) weaker than this result.

#### 4. CONCLUSIONS

In this paper we have presented the measurements of the parameters of  $\Lambda$ CDM,  $w_0$ CDM and  $w_0w_a$ CDM models from the full-shape power spectrum data, supplemented with the BBN, BAO and SNe measurements. Our constraints on the parameters of these models are significantly better than those based on the BAO data only, which clearly shows the statistical power of the effective field theory-based full-shape power spectrum likelihood [5, 19]. The measurements presented in this paper are also competitive with the Planck+BAO(+SNe) limits, especially for the dynamical dark energy model.

Importantly, the full-shape data allows us to place constraints on all relevant cosmological parameters of the considered non-minimal models. One of such parameters is the present-day Hubble constant  $H_0$ , which we measure to (1-2)% precision even in the extensions of  $\Lambda$ CDM. Remarkably, our results agree with the Planck-preferred results. This is an important test, showing good agreement between various data sets: the CMB [1, 50], large-scale structure [5, 6, 41, 43, 44, 51], the local measurements from the tip of the red giants branch [52], and strong lensing time-delays (after taking into account the mass-sheet degeneracy) [53]. These estimates, however, are still in tension with Cepheid-calibrated supernovae measurements, see [48] and references therein.

Our results have some implications for the so-called  $\sigma_8$ -tension [54], the apparent disagreement on the value of  $\sigma_8$  between Planck on one side and various large scale structure measurements on the other side, e.g. weak lensing measurements by the Dark Energy Survey [55] and Kilo-Degree Survey [56]. In all models that we consid-

ered, we found the mass fluctuation amplitude  $\sigma_8$  systematically lower than the Planck predictions for the same models, although the significance of this tension in terms of our error bars is quite low ( $< 2\sigma$ ). In order to draw more robust conclusions we need to reduce the statistical error of our measurement, which can be done either by including external data sets<sup>3</sup>, or collecting more data. The latter will certainly happen in the future with the Euclid [63, 64] and DESI [65] surveys, which promise to dramatically sharpen the precision of cosmological parameter measurements, see e.g. [66–70].

Overall, we have found no evidence for any of the extensions of the base  $\Lambda$ CDM model in our analysis of the FS+BAO+SNe data, which is fully independent from the Planck CMB anisotropies. Our analysis confirms a remarkably concordant picture of the universe, whose properties on a wide range of redshifts can be described within the simple flat  $\Lambda$ CDM model.

#### ACKNOWLEDGMENTS

We thank Oliver Philcox and Marko Simonovic for valuable discussions. The work is supported by the RFBR grant 20-02-00982. Our numerical calculations were partially performed on the Central Information and Computer Complex and heterogeneous computing platform HybriLIT at the supercomputer ‘Govorun’ in JINR.

Parameter estimates presented in this paper are obtained with the CLASS-PT Boltzmann code [19] (also see [37]) interfaced with the `Montepython` MCMC sampler [71, 72]. The plots with posterior densities and marginalized limits are generated with the latest version of the `getdist` package<sup>4</sup> [73], which is part of the `CosmoMC` code [74, 75].

We are grateful to Héctor Gil-Marín for making the Nseries mocks and related data products publicly available [76, 77].

<sup>3</sup> e.g. the bispectrum [57, 58], the void-galaxy correlation [59], or the counts-in-cells statistic [60–62].

<sup>4</sup> <https://getdist.readthedocs.io/en/latest/>

## Appendix A: Details of the full-shape likelihood and the hexadecapole moment

In this Appendix we discuss in detail the effective-field theory based full-shape power spectrum likelihood. We use the likelihood introduced in Ref. [9], but make several changes compared to the analysis of this paper. First, we use slightly different priors on the nuisance parameters. Second, we include the power spectrum hexadecapole moment  $\ell = 4$ . Third, as a result of including the hexadecapole, the posterior parameter volume shrinks, and the theory-systematic error becomes more sizeable. This motivates us to use a more conservative data cut compared to Ref. [9]. In what follows we validate the priors and data cuts used in our analysis.

The rationale behind the inclusion of the hexadecapole is the following one. The models that we consider in this paper mainly alter the background expansion and the growth of structures. These are probed through the distance measurements and redshift-space distortions [8]. The usual method to extract these quantities from the redshift-space power spectrum is the so-called alpha analysis, see Ref. [3] and Ref. [9] for a justification of this analysis in certain contexts. Ref. [3] has shown that the inclusion of the hexadecapole improves the distance and RSD measurements by  $\sim 30\%$ . Therefore, we expect that the hexadecapole should also shrink the parameter contours in the extended models that we consider here.

The caveat, however, is that the alpha-analysis does not rely on any physical model of the late-time expansion (though an early-universe model is still required in order to generate the power spectrum template). Therefore, the alpha-analysis does not respect relations between the radial and angular distances, which exist in particular models. This means that parts of the parameter space probed by the alpha-analysis can be unphysical. An example of this situation is the  $\Lambda$ CDM model, which, in fact, corresponds to an extremely narrow region of the parameter space probed by the alpha-analysis [9]. It can be that the physical priors on the distances diminish the information gain from the hexadecapole. Therefore, the natural question is whether the hexadecapole improves parameter constraints in the complete full-shape analysis done at the level of the physical models. Addressing this question is one of the goals of this section.

### 1. Nuisance parameters and priors

We fit the full-shape data with the one-loop perturbation theory model that is described by the following set of nuisance parameters (see [19] for details):

$$\{b_1, b_2, b_{\mathcal{G}_2}, b_{\Gamma_3}, c_0, c_2, \tilde{c}, P_{\text{shot}}, a_2\}, \quad (\text{A1})$$

where  $b_1$  is the linear galaxy bias,  $b_2$  is the local-density quadratic bias,  $b_{\mathcal{G}_2}$  and  $b_{\Gamma_3}$  are the quadratic and cubic tidal biases,  $c_0$  and  $c_2$  are the higher derivative biases for the monopole and quadrupole ( $k^2$ -counterterms),  $\tilde{c}$  is the higher-order  $k^4$  redshift-space counterterm,  $P_{\text{shot}}$  is the residual constant shot noise contribution and  $a_2$  is the scale-dependent redshift-space stochastic counterterm [79], which we define as

$$P_{\text{stoch,RSD}} = a_2 \left( \frac{k}{k_{\text{NL}}} \right)^2 \frac{1}{\bar{n}}, \quad (\text{A2})$$

where  $\bar{n}$  is the galaxy number-density and  $k_{\text{NL}}$  is the non-linear scale. The  $a_2$  counterterm was not used in Ref. [9] because it was found to be fully degenerate with  $\tilde{c}$  at the level of the monopole and quadrupole moments. The hexadecapole moment breaks this degeneracy. Even though we do not detect this coefficient, we prefer to scan over it in our MCMC chains because it affects the parameter error bars. We use the following priors on the nuisance parameters:

$$\begin{aligned} b_1 A^{1/2} &\in \text{flat}[1, 4], & b_2 A^{1/2} &\sim \mathcal{N}(0, 1^2), \\ b_{\mathcal{G}_2} A^{1/2} &\sim \mathcal{N}(0, 1^2), & b_{\Gamma_3} &\sim \mathcal{N}(0.65, 1^2), \\ c_0 &\sim \mathcal{N}(0, 30^2), & c_2 &\sim \mathcal{N}(30, 30^2) \\ \tilde{c} &\sim \mathcal{N}(500, 500^2), & P_{\text{shot}} &\sim \mathcal{N}(0, 5 \cdot 10^3), \end{aligned} \quad (\text{A3})$$

where  $A \equiv A_s/A_{s,\text{fid}}$  (see Eq. (A7)). The physical motivation behind the choice of our priors can be found in Refs. [19, 21]. As far as  $a_2$  is concerned, we set the following physical prior, see Eq. (A2):

$$\begin{aligned} a_2 &\sim \mathcal{N}(0, 2^2), \text{ with } k_{\text{NL}} = 0.45 \text{ hMpc}^{-1}, \\ \bar{n}^{-1} &= 5 \cdot 10^3 \text{ [h}^{-1}\text{Mpc]}^3. \end{aligned} \quad (\text{A4})$$

We set the scale-dependent stochastic counterterm  $a_0 = 0$  as suggested by the field level analysis of the BOSS-like dark matter halos [80].

Note that unlike the reference [9], we marginalize over  $b_{\Gamma_3}$  assuming a prior centered at the prediction of the coevolution model and with unit variance [81]. Fixing  $b_{\Gamma_3}$  or marginalizing over it does not have an impact

Dataset Param.	BOSS volume	10xBOSS volume
$\Delta\omega_{cdm}/\omega_{cdm}$	$0.0370^{+0.086}_{-0.11}$	$0.0151^{+0.037}_{-0.046}$
$\Delta h/h$	$0.00599^{+0.019}_{-0.017}$	$0.00192^{+0.0069}_{-0.0068}$
$\Delta n_s/n_s$	$-0.015^{+0.074}_{-0.074}$	$-0.0039^{+0.031}_{-0.028}$
$\Delta A_s/A_s$	$-0.0243^{+0.12}_{-0.18}$	$0.0239^{+0.070}_{-0.070}$
$\Delta \ln(10^{10} A_s)/\ln(10^{10} A_s)$	$-0.0119^{+0.053}_{-0.053}$	$0.0069^{+0.022}_{-0.022}$
$\Delta\Omega_m/\Omega_m$	$0.0181^{+0.060}_{-0.072}$	$0.0086^{+0.024}_{-0.029}$
$\Delta\sigma_8/\sigma_8$	$-0.0016^{+0.056}_{-0.062}$	$0.0188^{+0.022}_{-0.022}$

TABLE II. Mean values and 68% CL minimum credible intervals for the parameters of  $\Lambda$ CDM model inferred from the PT Challenge simulation spectra at  $z = 0.61$  for two choices of the covariance matrix, corresponding to the cumulative BOSS volume (2nd column) and 10 times the BOSS volume (3rd column). We display all parameters as  $(p - p_{\text{fid}})/p_{\text{fid}}$ , where  $p_{\text{fid}}$  is the fiducial value used in simulations. The top group represents the parameters that were directly varied in the MCMC chains. The bottom group are the derived parameters.

on our constraints [21]. Nevertheless, we prefer to do a marginalization over this unknown coefficient within a physically-motivated prior in order to be rigorous.

## 2. Validation on mock catalogs

The pipeline used in our work was already validated in Refs. [9, 78]. However, these works did not include the hexadecapole moment, which can change the conclusions on the data cut  $k_{\text{max}}$  used in the analysis. To check this, we test our pipeline on mock catalogs of the BOSS-like luminous red galaxies in this section in two different regimes. As a first step, we will fit the mock data from the periodic box N-body simulations PT Challenge (‘perturbation theory challenge’) [78]. As a second step, we will analyze the mock data from more realistic mock catalogs that include the survey mask and selection functions.

### a. Test on PT Challenge simulations

The PT challenge simulation suite was designed for testing perturbation theory modeling at the sub-percent level. These N-body simulations reproduce the clustering of the BOSS-like galaxies from the DR12 sample, in a gigantic cumulative volume of  $\sim 560$  (Gpc/h) $^3$ .

We will fit the data vector including the monopole, quadrupole and hexadecapole,  $\{P_0, P_2, P_4\}$  taken from a snapshot at  $z = 0.61$ , which corresponds to the high-

$z$  NGC sample, which is the most constraining BOSS data chunk. We use the mean data vector corresponding to the total simulation volume, but analyze it using a covariance which corresponds to the actual BOSS survey. In particular, we assume a Gaussian covariance for the power spectrum multipoles, with the following volumes and shot noise,

$$\begin{aligned} \text{BOSS-like : } \bar{n}^{-1} &= 5 \cdot 10^3 \text{ [Mpc/h]}^3, \quad V = 6 \text{ (Gpc/h)}^3, \\ \text{10x BOSS-like : } \bar{n}^{-1} &= 5 \cdot 10^3 \text{ [Mpc/h]}^3, \quad V = 60 \text{ (Gpc/h)}^3. \end{aligned} \quad (\text{A5})$$

The first choice corresponds to the cumulative volume of the BOSS survey. The second covariance corresponds to future surveys like DESI [65] and this case provides a more stringent test of our theory model, which will also be important in order to quantify the impact of the Bayesian parameter volume effects. We choose the data cut  $k_{\text{max}} = 0.2$  h/Mpc.

Our fitting model is characterized by the cosmological parameters of the base  $\Lambda$ CDM model,

$$\{\omega_{cdm}, n_s, h, A_s\}, \quad (\text{A6})$$

and we fix the baryon density  $\omega_b$  to the fiducial value in order to simulate the BBN prior. We will also use the following convenient amplitude parameter

$$A \equiv \frac{A_s}{A_{s, \text{fid}}}, \quad A_{s, \text{fid}} = 2.2109 \cdot 10^{-9} \quad (\text{A7})$$

During our MCMC analysis, we compute our theoretical templates with CLASS-PT [19]. It should be mentioned

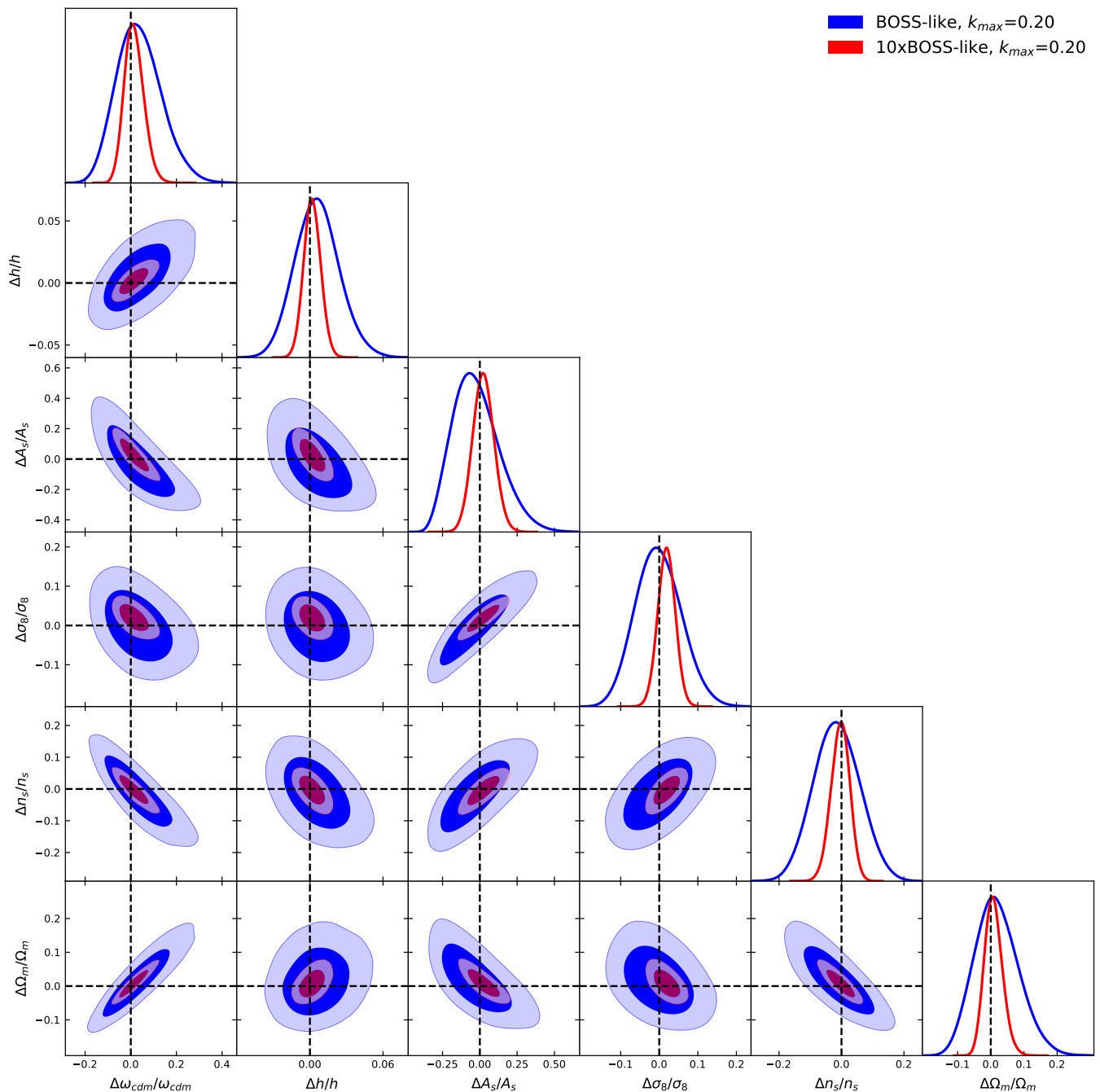


FIG. 4. Posterior distributions of the cosmological parameters of the  $\Lambda$ CDM model fitted to the PT Challenge mock data [78]. All parameters are normalized to represent the relative deviations from the fiducial values used in the N-body simulations.

that our current one-loop calculation is based on the Einstein-de-Sitter approximation, which has been shown to be accurate both in  $\Lambda$ CDM and its extensions [82].

The results of our analysis are shown in Fig. 4 and in Table II. As the perturbation theory challenge is still ongoing, we display the parameters normalized to the fidu-

cial values in order to keep the true cosmology blinded.

Let us first look at the BOSS-like case. We see that our pipeline reproduces the true value of cosmological parameters to percent and sub-percent precision. Moreover, we find the error bars that are very similar to the actual error bars from the analysis of the full BOSS

Param.	fiducial	$P_{0,2} (k_{\max} = 0.2)$	$P_{0,2,4} (k_{\max} = 0.2)$	$P_{0,2} (k_{\max} = 0.25)$	$P_{0,2,4} (k_{\max} = 0.25)$
$\omega_{cdm}$	0.117	$0.125^{+0.010}_{-0.013}$	$0.123^{+0.009}_{-0.011}$	$0.122^{+0.010}_{-0.013}$	$0.119^{+0.007}_{-0.011}$
$h$	0.7	$0.707^{+0.015}_{-0.016}$	$0.707^{+0.012}_{-0.013}$	$0.706^{+0.015}_{-0.016}$	$0.702^{+0.011}_{-0.013}$
$A$	1	$0.941^{+0.139}_{-0.202}$	$1.022^{+0.134}_{-0.184}$	$1.013^{+0.153}_{-0.204}$	$1.157^{+0.152}_{-0.175}$
$n_s$	0.96	$0.920^{+0.071}_{-0.071}$	$0.941^{+0.066}_{-0.064}$	$0.918^{+0.072}_{-0.067}$	$0.950^{+0.061}_{-0.052}$
$\Omega_m$	0.286	$0.297^{+0.017}_{-0.019}$	$0.292^{+0.014}_{-0.016}$	$0.291^{+0.015}_{-0.018}$	$0.289^{+0.011}_{-0.014}$
$\sigma_8$	0.82	$0.812^{+0.062}_{-0.067}$	$0.845^{+0.051}_{-0.056}$	$0.828^{+0.058}_{-0.060}$	$0.885^{+0.046}_{-0.045}$

TABLE III. The marginalized 1d intervals for the cosmological parameters estimated from the Nseries mock data at  $z_{\text{eff}} = 0.55$ . The shown are the fitted parameters (first column), fiducial values used in simulations (second column), the results for  $P_0 + P_2$  (third column) and  $P_0 + P_2 + P_4$  (fourth column) both at  $k_{\max} = 0.20h\text{Mpc}^{-1}$ , along with the same combinations at  $k_{\max} = 0.25h\text{Mpc}^{-1}$  (fifth and sixth columns).

data. The shifts in the relevant cosmological parameters  $\{\omega_{cdm}, n_s, h, \ln(10^{10}A_s), \sigma_8, \Omega_m\}$  are

$$\{3.7, -1.5, 0.6, -1.1, -0.16, 1.8\} \%,$$

or

$$\{0.37, -0.2, 0.33, -0.21, -0.027, 0.27\} \sigma$$

if formulated in terms of the standard deviations.

Part of these shifts is produced by marginalization effects. Even though these effects are present in the data as well, it is instructive to perform an analysis with a smaller covariance in order to get an idea on their size. For the 10xBOSS case, the shifts are

$$\{1.5, -0.39, 0.19, 0.69, 1.9, 0.86\} \%$$

or

$$\{0.15, -0.05, 0.1, 0.13, 0.32, 0.13\} \sigma$$

if formulated in terms of the error bars of the actual BOSS analysis. We conclude that for the survey of the BOSS volume the parameter volume effects represent the dominant part of the apparent shift of cosmological parameters from the true values. The marginalization effects affect the posteriors of all cosmological parameters at the level of  $0.3\sigma$ . The true theory-systematic shifts due to higher-order non-linear corrections are very marginal, the largest one is in  $\sigma_8$  and it has  $0.3\sigma$  significance.

#### b. Test on Nseries simulations

As a second test, we validate our pipeline on the Nseries cut-sky mock catalogs, which closely reproduce

the actual BOSS CMASS sample (largely overlapping with the NGC high-z footprint used in our main analysis), including the appropriate survey geometry and selection functions. These mocks are based on full N-body simulations and hence accurately reproduce the dynamics of gravitation clustering. The details of the mocks are given in Ref. [18]. These mocks were generated for the following fiducial cosmology:  $\Omega_m = 0.286$ ,  $\Omega_b = 0.047$  ( $\Omega_b h^2 = 0.023$ ),  $\ln(10^{10}A_s) = 3.065$ ,  $n_s = 0.96$ ,  $\sigma_8 = 0.82$ , and  $h = 0.7$ . The resulting spectra for Nseries have been obtained assuming a fiducial matter abundance  $\Omega_m = 0.31$  when converting redshifts and angles into comoving distances. The same fiducial matter abundance was used in the actual BOSS data and in our theoretical templates, which include the Alcock-Paczynski effect. The effective redshift is  $z_{\text{eff}} = 0.55$ .

We use the data vector averaged over 84 cut-sky realizations to suppress the statistical fluctuations. The data is analyzed using the covariance matrix from the Patchy mocks, which corresponds to the BOSS CMASS NGC sample. We decided to not use Nseries mock data to build the covariance for the following two reasons. First, the Patchy mocks reproduce the BOSS CMASS NGC sample that guarantees the same parameter volume effects as the analysis of the real data. Second, Nseries sample does not include veto effect which was imprinted into the Patchy mocks and real data. Since our goal is to validate the theoretical framework on the real data, we extract the covariance from the NGC Patchy mock and not from different realizations of the Nseries mocks.

All in all, the Nseries simulations reproduce general characteristics of the BOSS CMASS NGC sample, which

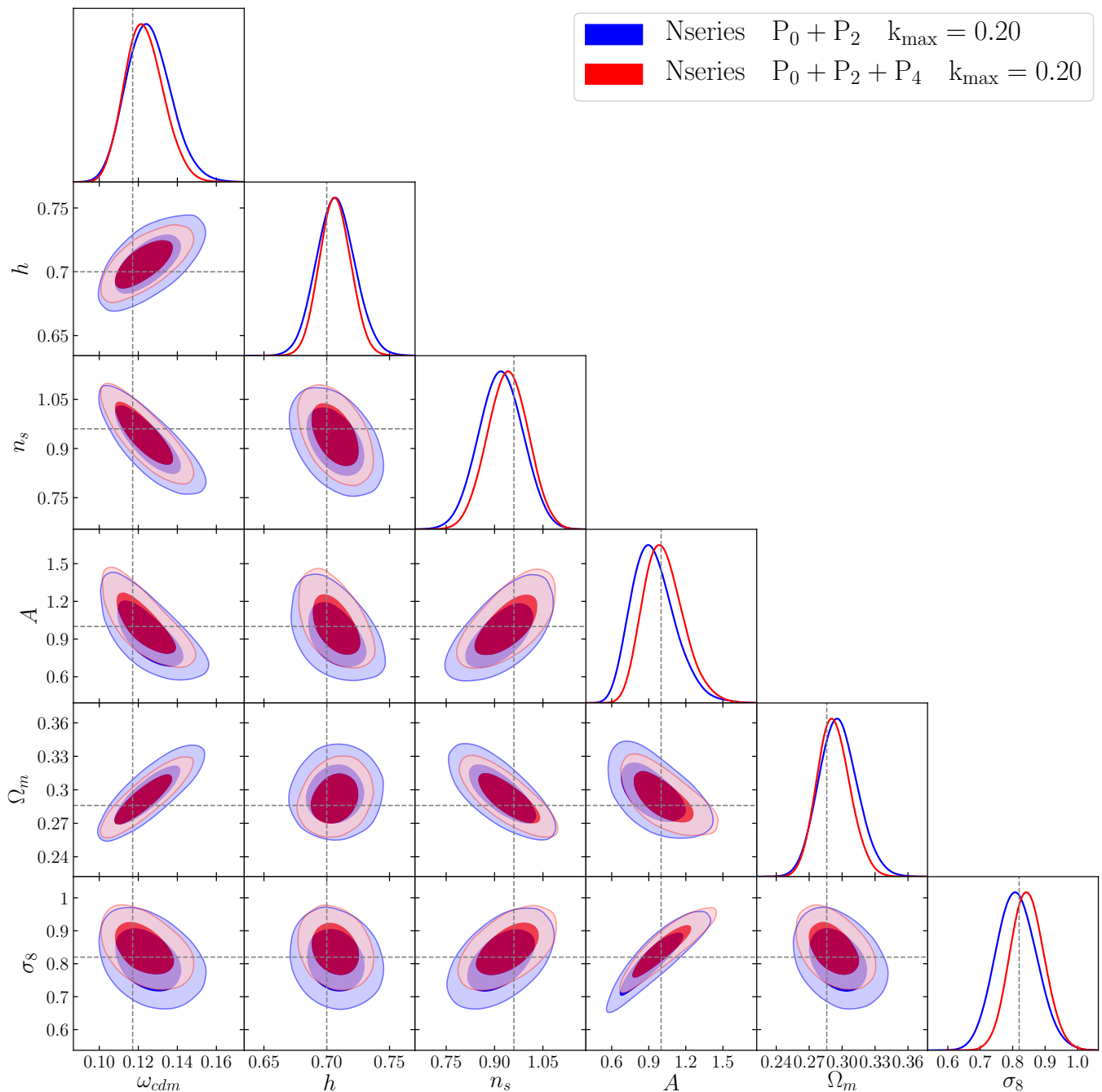


FIG. 5. Posterior distributions of the cosmological parameters of the  $\Lambda$ CDM model fitted to the Nseries mock data for  $k_{\max} = 0.2h\text{Mpc}^{-1}$ .

has effective tomographic volume  $2.8 (\text{Gpc}/h)^3$ . The inverse number density for these mocks is

$$\bar{n}^{-1} = 5.3 \cdot 10^3 [\text{Mpc}/h]^3. \quad (\text{A8})$$

Since the mocks have a non-trivial mask, we convolve the theoretical spectra with the survey window function as prescribed by Ref. [3].

The results of our analysis are shown in Fig. 5 (for  $k_{\max} = 0.2 h/\text{Mpc}$ ), and Fig. 6 (for  $k_{\max} = 0.25 h/\text{Mpc}$ ). 1d marginalized limits are given in Table III.

Let us first focus on the data cut  $k_{\max} = 0.2 h\text{Mpc}^{-1}$ . From Fig. 5 we see that our pipeline gives unbiased results with or without the hexadecapole moment at this

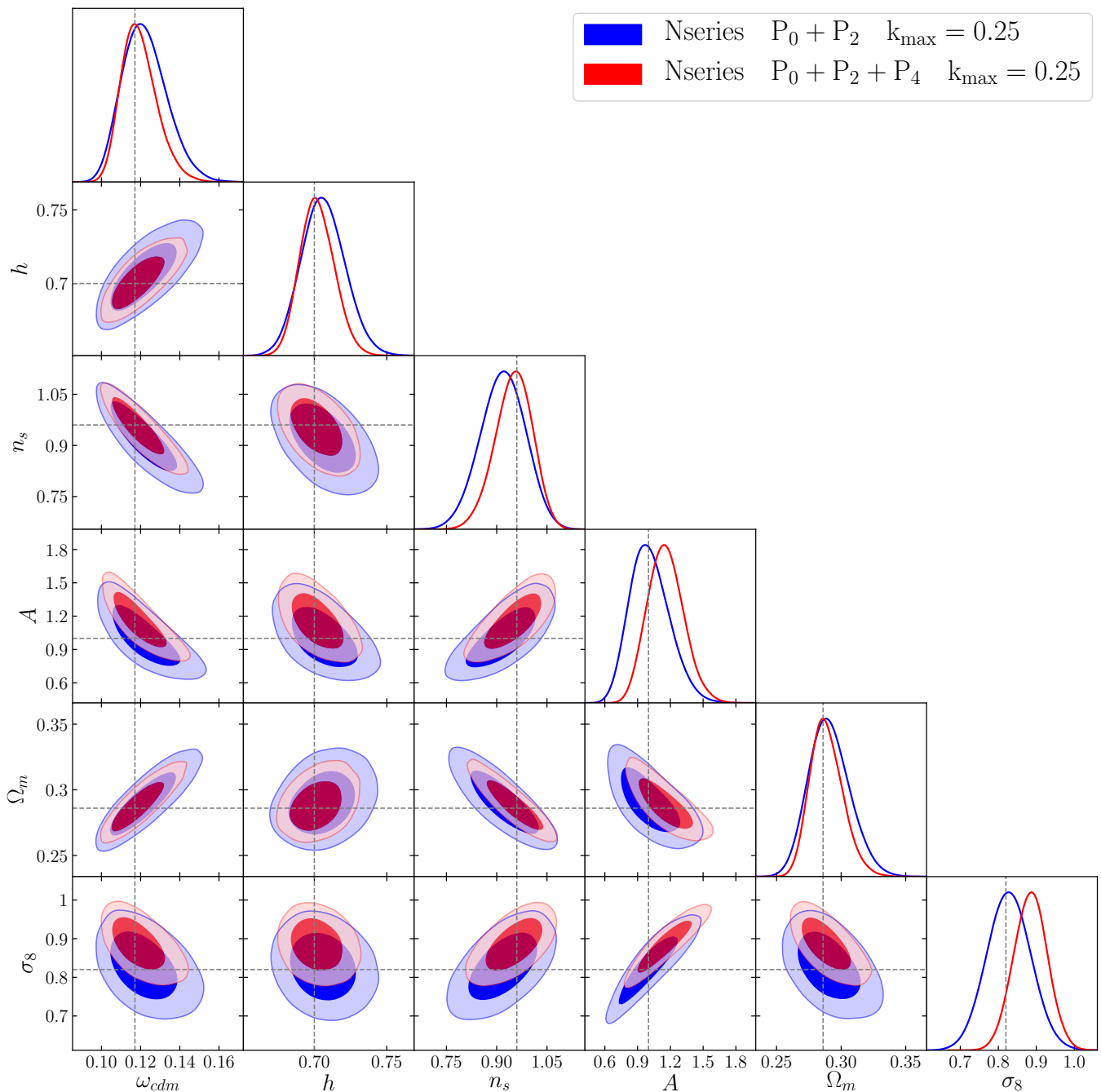


FIG. 6. Posterior distributions of the cosmological parameters of the  $\Lambda$ CDM model fitted to the Nseries mock data for  $k_{\max} = 0.25h\text{Mpc}^{-1}$ .

data cut. The shifts between the means and the true values of cosmological parameters are  $\lesssim 0.5\sigma$ , consistent with the marginalization effects found earlier in the analysis of the PT challenge data.

Now let us consider a more aggressive data cut  $k_{\max} = 0.25 h/\text{Mpc}$ . In this case, the addition of the hexade-

capole shrinks the parameter error bars such that the results at  $k_{\max} = 0.25 h/\text{Mpc}$  (which was the baseline data cut in Ref. [9]) become biased. Indeed, looking at Fig. 6 we see that the true cosmology is beyond the 95% confidence interval in the 2d space  $\sigma_8 - \Omega_m$ , which is not the case for the  $P_{0,2}$  analysis. This is the main reason why

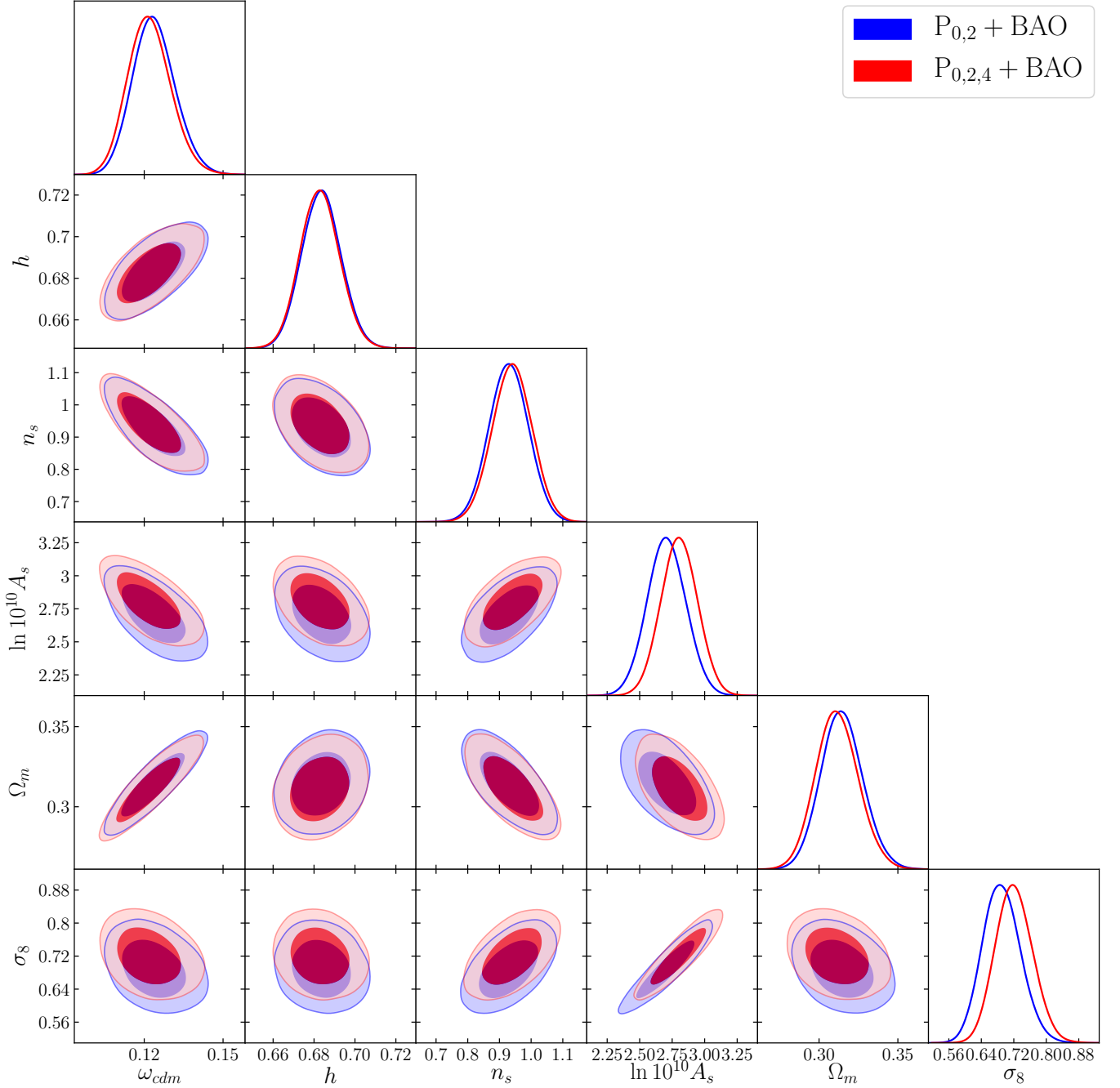


FIG. 7. Posterior distributions of the cosmological parameters of the  $\Lambda$ CDM model inferred without and with the hexadecapole.

we chose a more conservative data cut  $k_{\max} = 0.2 \text{ h/Mpc}$  in the baseline analysis of this paper. Importantly, the error bars in the case  $P_{0,2,4}$  at  $k_{\max} = 0.2 \text{ hMpc}^{-1}$  are smaller than the error bars in the case  $P_{0,2}$  at  $k_{\max} = 0.25 \text{ hMpc}^{-1}$ , which suggests that it is more beneficial to include the hexadecapole at  $k_{\max} = 0.2 \text{ hMpc}^{-1}$  than

pushing to  $k_{\max} = 0.25 \text{ hMpc}^{-1}$  with the monopole and quadrupole only.

All in all, the results of this section imply that  $k_{\max} = 0.2 \text{ hMpc}^{-1}$  is a reasonable data cut, for which the total systematic error, including the modeling uncertainties and marginalization effects, is smaller than the statistical

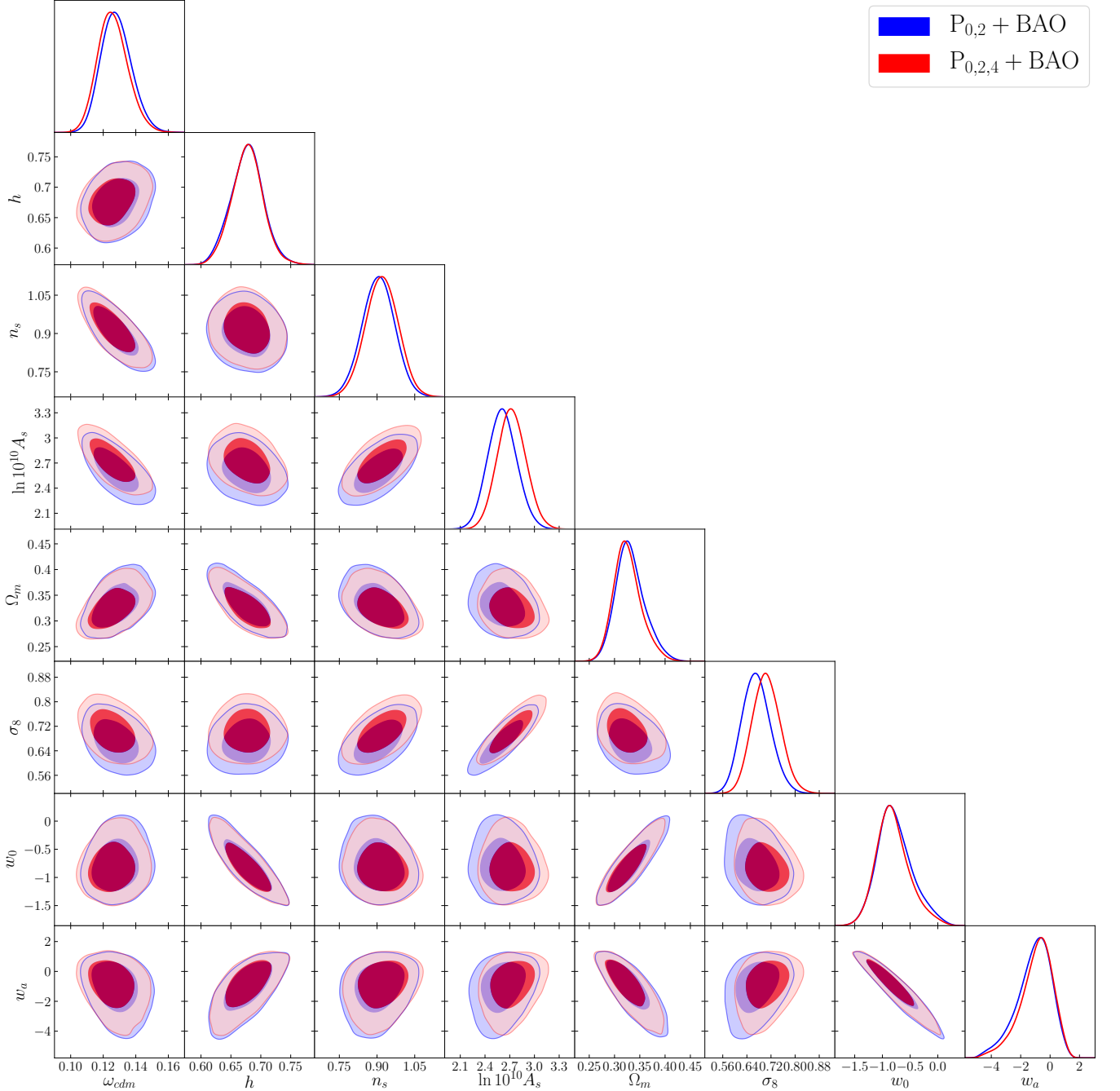


FIG. 8. Posterior distributions of the cosmological parameters of the  $w_0w_a$ CDM model inferred without and with the hexadecapole.

error.

### 3. Cosmological information from the hexadecapole

It is instructive to quantify how much the power spectrum hexadecapole improves the parameter constraints

compared to the monopole and quadrupole combination. To that end we analyze the BOSS FS data using two different data vectors,  $P_0 + P_0$  and  $P_0 + P_2 + P_4$ , both at  $k_{\max} = 0.2 \text{ hMpc}^{-1}$ , and including the BAO data along with the BBN prior on  $\omega_b$ .

Let us first focus on the base  $\Lambda$ CDM model. The re-

Param.	$\Lambda$ CDM, $P_{0,2}$	$\Lambda$ CDM, $P_{0,2,4}$	$w_0w_a$ CDM, $P_{0,2}$	$w_0w_a$ CDM, $P_{0,2,4}$
$\omega_{\text{cdm}}$	$0.1237^{+0.0077}_{-0.0087}$	$0.1221^{+0.0074}_{-0.0089}$	$0.1283^{+0.0082}_{-0.01}$	$0.126^{+0.0085}_{-0.01}$
$h$	$0.6836^{+0.0096}_{-0.0099}$	$0.683^{+0.0095}_{-0.0099}$	$0.6767^{+0.027}_{-0.028}$	$0.6775^{+0.026}_{-0.026}$
$\ln(10^{10} A_s)$	$2.71^{+0.15}_{-0.15}$	$2.80^{+0.14}_{-0.14}$	$2.61^{+0.18}_{-0.18}$	$2.72^{+0.17}_{-0.17}$
$n_s$	$0.9305^{+0.062}_{-0.064}$	$0.9401^{+0.063}_{-0.062}$	$0.904^{+0.067}_{-0.061}$	$0.9191^{+0.066}_{-0.065}$
$w_0$	—	—	$-0.7618^{+0.26}_{-0.36}$	$-0.805^{+0.25}_{-0.34}$
$w_a$	—	—	$-1.141^{+1.4}_{-0.84}$	$-0.9451^{+1.3}_{-0.83}$
$\Omega_{\text{de}}$	—	—	$0.668^{+0.033}_{-0.024}$	$0.673^{+0.031}_{-0.022}$
$\Omega_m$	$0.3145^{+0.013}_{-0.014}$	$0.3116^{+0.013}_{-0.014}$	$0.3322^{+0.024}_{-0.033}$	$0.3262^{+0.023}_{-0.031}$
$\sigma_8$	$0.691^{+0.043}_{-0.050}$	$0.720^{+0.042}_{-0.047}$	$0.673^{+0.043}_{-0.050}$	$0.705^{+0.044}_{-0.049}$
$r_d$ [Mpc]	$145^{+2.4}_{-2.4}$	$145^{+2.4}_{-2.4}$	$145^{+2.4}_{-2.4}$	$145^{+2.4}_{-2.4}$

TABLE IV. The marginalized 1d intervals for the cosmological parameters estimated from the BBN+FS+BAO likelihood. We show the results for  $\Lambda$ CDM (second and third columns) and for the  $w_0w_a$ CDM model (fourth and fifth columns). In either case we display the results obtained with and without the hexadecapole moment.

sults of our analysis are displayed in Fig. 7 and in Table IV. We see that the hexadecapole does not noticeably improve the parameter constraints. The only result of the inclusion the hexadecapole moment is a marginal upward shift of  $\sigma_8$ . The same tendency has been found in the results with the Nseries mocks which reliably describe the survey geometry and selection functions, see Sec. A 2 b. This effect can be attributed to the reduction of the parameter volume effect, which also brings the amplitude closer to the Planck prediction. All in all, we find the inclusion of the hexadecapole reduces the total volume in cosmological parameter space by 2% compared to the monopole and quadrupole analysis in the base  $\Lambda$ CDM model.

Now let us focus on the  $w_0w_a\Lambda$ CDM model. This model has a larger number of free parameters and hence we expect the gain from the hexadecapole to be more significant here. However, looking at Fig. 8 and in Table IV, we see that the improvement is quite marginal here. This result should be contrasted with the claims of

Ref. [3] that the hexadecapole improves the constraints on the distance parameters inferred through the so-called alpha-analysis. Having repeated this analysis we have indeed reproduced the same  $\sim 30\%$  improvement with our theoretical model and scale cuts. However, we see that this gain does not propagate into the actual physical parameters even in the extended  $w_0w_a\Lambda$ CDM model. It remains to be seen if the improvement from the hexadecapole reported in Ref. [3] is merely an artifact of the scaling alpha-analysis, which does not correspond to any physical model.

Even though the effect of the hexadecapole on the 1d parameter constraints is quite marginal, it should be mentioned that it decreases the total volume of the 2d posterior  $w_0 - w_a$  by 19% as compared to the  $P_{0,2}$  combination. The addition of the hexadecapole seems to be more beneficial if we consider the total posterior volume of all sampled cosmological parameters, which reduces by 26%. Thus, the 1d marginalized limits might not fully reflect the information content of the hexadecapole.

---

[1] N. Aghanim *et al.* (Planck), (2018), [arXiv:1807.06209 \[astro-ph.CO\]](#).  
[2] N. Aghanim *et al.* (Planck), (2019), [arXiv:1907.12875 \[astro-ph.CO\]](#).  
[3] F. Beutler *et al.* (BOSS), *Mon. Not. Roy. Astron. Soc.* **466**, 2242 (2017), [arXiv:1607.03150 \[astro-ph.CO\]](#).

[4] C. Alcock and B. Paczynski, *Nature* **281**, 358 (1979).  
[5] M. M. Ivanov, M. Simonović, and M. Zaldarriaga, *JCAP* **05**, 042 (2020), [arXiv:1909.05277 \[astro-ph.CO\]](#).  
[6] G. D’Amico, J. Gleyzes, N. Kokron, D. Markovic, L. Senatore, P. Zhang, F. Beutler, and H. Gil-Marín, (2019), [arXiv:1909.05271 \[astro-ph.CO\]](#).

- [7] T. Colas, G. D’amico, L. Senatore, P. Zhang, and F. Beutler, *JCAP* **06**, 001 (2020), [arXiv:1909.07951 \[astro-ph.CO\]](#).
- [8] S. Alam *et al.* (BOSS), *Mon. Not. Roy. Astron. Soc.* **470**, 2617 (2017), [arXiv:1607.03155 \[astro-ph.CO\]](#).
- [9] M. M. Ivanov, M. Simonović, and M. Zaldarriaga, *Phys. Rev. D* **101**, 083504 (2020), [arXiv:1912.08208 \[astro-ph.CO\]](#).
- [10] O. H. Philcox, B. D. Sherwin, G. S. Farren, and E. J. Baxter, (2020), [arXiv:2008.08084 \[astro-ph.CO\]](#).
- [11] G. D’Amico, L. Senatore, and P. Zhang, (2020), [arXiv:2003.07956 \[astro-ph.CO\]](#).
- [12] M. M. Ivanov, E. McDonough, J. C. Hill, M. Simonović, M. W. Toomey, S. Alexander, and M. Zaldarriaga, (2020), [arXiv:2006.11235 \[astro-ph.CO\]](#).
- [13] G. D’Amico, L. Senatore, P. Zhang, and H. Zheng, (2020), [arXiv:2006.12420 \[astro-ph.CO\]](#).
- [14] E. Di Valentino, A. Melchiorri, and J. Silk, *Nature Astron.* **4**, 196 (2019), [arXiv:1911.02087 \[astro-ph.CO\]](#).
- [15] P. A. R. Ade *et al.* (Planck), *Astron. Astrophys.* **594**, A13 (2016), [arXiv:1502.01589 \[astro-ph.CO\]](#).
- [16] G. E. Addison, Y. Huang, D. J. Watts, C. L. Bennett, M. Halpern, G. Hinshaw, and J. L. Weiland, *Astrophys. J.* **818**, 132 (2016), [arXiv:1511.00055 \[astro-ph.CO\]](#).
- [17] N. Aghanim *et al.* (Planck), *Astron. Astrophys.* **607**, A95 (2017), [arXiv:1608.02487 \[astro-ph.CO\]](#).
- [18] N. Hand, Y. Feng, F. Beutler, Y. Li, C. Modi, U. Seljak, and Z. Slepian, *Astron. J.* **156**, 160 (2018), [arXiv:1712.05834 \[astro-ph.IM\]](#).
- [19] A. Chudaykin, M. M. Ivanov, O. H. Philcox, and M. Simonović, (2020), [arXiv:2004.10607 \[astro-ph.CO\]](#).
- [20] F.-S. Kitaura *et al.*, *Mon. Not. Roy. Astron. Soc.* **456**, 4156 (2016), [arXiv:1509.06400 \[astro-ph.CO\]](#).
- [21] D. Wadekar, M. M. Ivanov, and R. Scoccimarro, (2020), [arXiv:2009.00622 \[astro-ph.CO\]](#).
- [22] O. H. Philcox, M. M. Ivanov, M. Zaldarriaga, M. Simonovic, and M. Schmittfull, (2020), [arXiv:2009.03311 \[astro-ph.CO\]](#).
- [23] F. Beutler *et al.* (BOSS), *Mon. Not. Roy. Astron. Soc.* **464**, 3409 (2017), [arXiv:1607.03149 \[astro-ph.CO\]](#).
- [24] O. H. Philcox, M. M. Ivanov, M. Simonović, and M. Zaldarriaga, *JCAP* **05**, 032 (2020), [arXiv:2002.04035 \[astro-ph.CO\]](#).
- [25] T. Baldauf, M. Mirbabayi, M. Simonović, and M. Zaldarriaga, (2016), [arXiv:1602.00674 \[astro-ph.CO\]](#).
- [26] A. J. Ross, L. Samushia, C. Howlett, W. J. Percival, A. Burden, and M. Manera, *Mon. Not. Roy. Astron. Soc.* **449**, 835 (2015), [arXiv:1409.3242 \[astro-ph.CO\]](#).
- [27] F. Beutler, C. Blake, M. Colless, D. Jones, L. Staveley-Smith, L. Campbell, Q. Parker, W. Saunders, and F. Watson, *Mon. Not. Roy. Astron. Soc.* **416**, 3017 (2011), [arXiv:1106.3366 \[astro-ph.CO\]](#).
- [28] H. du Mas des Bourboux *et al.*, (2020), [arXiv:2007.08995 \[astro-ph.CO\]](#).
- [29] S. Alam *et al.* (eBOSS), (2020), [arXiv:2007.08991 \[astro-ph.CO\]](#).
- [30] R. Neveux *et al.*, (2020), [arXiv:2007.08999 \[astro-ph.CO\]](#).
- [31] A. de Mattia *et al.*, (2020), [arXiv:2007.09008 \[astro-ph.CO\]](#).
- [32] H. Gil-Marín *et al.*, (2020), [arXiv:2007.08994 \[astro-ph.CO\]](#).
- [33] D. Scolnic *et al.*, *Astrophys. J.* **859**, 101 (2018), [arXiv:1710.00845 \[astro-ph.CO\]](#).
- [34] E. Aver, K. A. Olive, and E. D. Skillman, *JCAP* **07**, 011 (2015), [arXiv:1503.08146 \[astro-ph.CO\]](#).
- [35] R. J. Cooke, M. Pettini, and C. C. Steidel, *Astrophys. J.* **855**, 102 (2018), [arXiv:1710.11129 \[astro-ph.CO\]](#).
- [36] D. J. Fixsen, E. S. Cheng, J. M. Gales, J. C. Mather, R. A. Shafer, and E. L. Wright, *Astrophys. J.* **473**, 576 (1996), [arXiv:astro-ph/9605054 \[astro-ph\]](#).
- [37] D. Blas, J. Lesgourgues, and T. Tram, *JCAP* **1107**, 034 (2011), [arXiv:1104.2933 \[astro-ph.CO\]](#).
- [38] M. M. Ivanov, Y. Ali-Haïmoud, and J. Lesgourgues, *Phys. Rev. D* **102**, 063515 (2020), [arXiv:2005.10656 \[astro-ph.CO\]](#).
- [39] V. F. Mukhanov, *Int. J. Theor. Phys.* **43**, 623 (2004), [arXiv:astro-ph/0303072](#).
- [40] M. Tegmark *et al.* (SDSS), *Phys. Rev. D* **74**, 123507 (2006), [arXiv:astro-ph/0608632](#).
- [41] E. Aubourg *et al.*, *Phys. Rev. D* **92**, 123516 (2015), [arXiv:1411.1074 \[astro-ph.CO\]](#).
- [42] M. Zaldarriaga, D. N. Spergel, and U. Seljak, *Astrophys. J.* **488**, 1 (1997), [arXiv:astro-ph/9702157](#).
- [43] A. Cuceu, J. Farr, P. Lemos, and A. Font-Ribera, *JCAP* **10**, 044 (2019), [arXiv:1906.11628 \[astro-ph.CO\]](#).
- [44] N. Schöneberg, J. Lesgourgues, and D. C. Hooper, *JCAP* **10**, 029 (2019), [arXiv:1907.11594 \[astro-ph.CO\]](#).
- [45] A. Obuljen, W. J. Percival, and N. Dalal, (2020), [arXiv:2004.07240 \[astro-ph.CO\]](#).
- [46] E. Di Valentino *et al.*, (2020), [arXiv:2008.11286 \[astro-ph.CO\]](#).
- [47] A. G. Riess, S. Casertano, W. Yuan, L. M. Macri, and D. Scolnic, *Astrophys. J.* **876**, 85 (2019), [arXiv:1903.07603 \[astro-ph.CO\]](#).
- [48] E. Di Valentino *et al.*, (2020), [arXiv:2008.11284 \[astro-ph.CO\]](#).
- [49] “Planck 2018: Cosmological parameter tables,” [https://wiki.cosmos.esa.int/planck-legacy-archive/images/b/be/Baseline\\_params\\_table\\_2018\\_68pc.pdf](https://wiki.cosmos.esa.int/planck-legacy-archive/images/b/be/Baseline_params_table_2018_68pc.pdf).
- [50] S. Aiola *et al.* (ACT), (2020), [arXiv:2007.07288 \[astro-ph.CO\]](#).

- [51] T. Abbott *et al.* (DES), *Mon. Not. Roy. Astron. Soc.* **480**, 3879 (2018), [arXiv:1711.00403 \[astro-ph.CO\]](#).
- [52] W. L. Freedman *et al.*, (2019), [10.3847/1538-4357/ab2f73](#), [arXiv:1907.05922 \[astro-ph.CO\]](#).
- [53] S. Birrer *et al.*, (2020), [arXiv:2007.02941 \[astro-ph.CO\]](#).
- [54] E. Di Valentino *et al.*, (2020), [arXiv:2008.11285 \[astro-ph.CO\]](#).
- [55] T. M. C. Abbott *et al.* (DES), *Phys. Rev.* **D98**, 043526 (2018), [arXiv:1708.01530 \[astro-ph.CO\]](#).
- [56] C. Heymans, T. Tröster, M. Asgari, C. Blake, H. Hildebrandt, B. Joachimi, K. Kuijken, C.-A. Lin, A. G. Sánchez, J. L. van den Busch, A. H. Wright, A. Amon, M. Bilicki, J. de Jong, M. Crocce, A. Dvornik, T. Erben, F. Getman, B. Giblin, K. Glazebrook, H. Hoekstra, S. Joudaki, A. Kannawadi, C. Lidman, F. Köhlinger, L. Miller, N. R. Napolitano, D. Parkinson, P. Schneider, H. Shan, and C. Wolf, *arXiv e-prints*, [arXiv:2007.15632](#) (2020), [arXiv:2007.15632 \[astro-ph.CO\]](#).
- [57] H. Gil-Marín, J. Noreña, L. Verde, W. J. Percival, C. Wagner, M. Manera, and D. P. Schneider, *Mon. Not. Roy. Astron. Soc.* **451**, 539 (2015), [arXiv:1407.5668 \[astro-ph.CO\]](#).
- [58] H. Gil-Marín, W. J. Percival, L. Verde, J. R. Brownstein, C.-H. Chuang, F.-S. Kitaura, S. A. Rodríguez-Torres, and M. D. Olmstead, *Mon. Not. Roy. Astron. Soc.* **465**, 1757 (2017), [arXiv:1606.00439 \[astro-ph.CO\]](#).
- [59] S. Nadathur *et al.*, (2020), [arXiv:2008.06060 \[astro-ph.CO\]](#).
- [60] C. Uhlemann, S. Codis, C. Pichon, F. Bernardeau, and P. Reimberg, *Mon. Not. Roy. Astron. Soc.* **460**, 1529 (2016), [arXiv:1512.05793 \[astro-ph.CO\]](#).
- [61] M. M. Ivanov, A. A. Kaurov, and S. Sibiryakov, *JCAP* **1903**, 009 (2019), [arXiv:1811.07913 \[astro-ph.CO\]](#).
- [62] A. Repp and I. Szapudi, (2020), [10.1093/mnras/laaa139](#), [arXiv:2006.01146 \[astro-ph.CO\]](#).
- [63] R. Laureijs *et al.* (EUCLID), (2011), [arXiv:1110.3193 \[astro-ph.CO\]](#).
- [64] L. Amendola *et al.*, *Living Rev. Rel.* **21**, 2 (2018), [arXiv:1606.00180 \[astro-ph.CO\]](#).
- [65] A. Aghamousa *et al.* (DESI), (2016), [arXiv:1611.00036 \[astro-ph.IM\]](#).
- [66] A. Chudaykin and M. M. Ivanov, *JCAP* **1911**, 034 (2019), [arXiv:1907.06666 \[astro-ph.CO\]](#).
- [67] B. Audren, J. Lesgourgues, S. Bird, M. G. Haehnelt, and M. Viel, *JCAP* **1301**, 026 (2013), [arXiv:1210.2194 \[astro-ph.CO\]](#).
- [68] T. Brinckmann, D. C. Hooper, M. Archidiacono, J. Lesgourgues, and T. Sprenger, *JCAP* **1901**, 059 (2019), [arXiv:1808.05955 \[astro-ph.CO\]](#).
- [69] A. Orsi, C. M. Baugh, C. G. Lacey, A. Cimatti, Y. Wang, and G. Zamorani, *Mon. Not. Roy. Astron. Soc.* **405**, 1006 (2010), [arXiv:0911.0669 \[astro-ph.CO\]](#).
- [70] V. Yankelevich and C. Porciani, *Mon. Not. Roy. Astron. Soc.* **483**, 2078 (2019), [arXiv:1807.07076 \[astro-ph.CO\]](#).
- [71] B. Audren, J. Lesgourgues, K. Benabed, and S. Prunet, *JCAP* **1302**, 001 (2013), [arXiv:1210.7183 \[astro-ph.CO\]](#).
- [72] T. Brinckmann and J. Lesgourgues, *Phys. Dark Univ.* **24**, 100260 (2019), [arXiv:1804.07261 \[astro-ph.CO\]](#).
- [73] A. Lewis, (2019), [arXiv:1910.13970 \[astro-ph.IM\]](#).
- [74] A. Lewis and S. Bridle, *Phys. Rev.* **D66**, 103511 (2002), [arXiv:astro-ph/0205436 \[astro-ph\]](#).
- [75] A. Lewis, *Phys. Rev.* **D87**, 103529 (2013), [arXiv:1304.4473 \[astro-ph.CO\]](#).
- [76] H. Gil-Marín *et al.*, *Mon. Not. Roy. Astron. Soc.* **460**, 4188 (2016), [arXiv:1509.06386 \[astro-ph.CO\]](#).
- [77] “Power spectrum and bispectrum files,” <http://icc.ub.edu/~hector/page10.html>.
- [78] T. Nishimichi, G. D’Amico, M. M. Ivanov, L. Senatore, M. Simonovic, M. Takada, M. Zaldarriaga, and P. Zhang, (2020), [arXiv:2003.08277 \[astro-ph.CO\]](#).
- [79] A. Perko, L. Senatore, E. Jennings, and R. H. Wechsler, (2016), [arXiv:1610.09321 \[astro-ph.CO\]](#).
- [80] M. Schmittfull, M. Simonović, V. Assassi, and M. Zaldarriaga, *Phys. Rev. D* **100**, 043514 (2019), [arXiv:1811.10640 \[astro-ph.CO\]](#).
- [81] V. Desjacques, D. Jeong, and F. Schmidt, *JCAP* **1812**, 035 (2018), [arXiv:1806.04015 \[astro-ph.CO\]](#).
- [82] Y. Donath and L. Senatore, (2020), [arXiv:2005.04805 \[astro-ph.CO\]](#).